

# Quantification of the morphology of sucrose crystals by image analysis

N. Faria<sup>a</sup>, M.N. Pons<sup>b,\*</sup>, S. Feyo de Azevedo<sup>a</sup>, F.A. Rocha<sup>a</sup>, H. Vivier<sup>c</sup>

<sup>a</sup>Departamento de Engenharia Química, Faculdade de Engenharia, Universidade do Porto, rua Roberto Frias s/n, 4200-465 Oporto, Portugal

<sup>b</sup>Laboratoire des Sciences du Génie Chimique, CNRS-ENSIC-INPL, 1, rue Grandville, BP 451, F-54001 Nancy cedex, France

<sup>c</sup>Laboratoire de Chimie et Environnement, Faculté des Sciences, 23, rue Paul Michelon, F-42023 Saint-Etienne cedex 2, France

Received 15 May 2002; received in revised form 24 February 2003; accepted 27 March 2003

## Abstract

Automated image analysis procedures combined with discriminant factorial analysis (DFA) have been developed to classify agglomerated sucrose crystals according to their shape. The crystals are observed by optical microscopy. Agreement between manual and automated classifications is 90% in average. Each crystal is characterised by its own degree of agglomeration, calculated from the output of the classification. Mono-crystals are further classified into two types according to the habit of their projected silhouette. The use of these techniques is illustrated on commercial sucrose and batch-crystallised particles obtained in a lab-scale reactor in presence of impurities (dextran, raffinose, glucose, sodium carbonate) known to modify the sucrose crystal habit.

© 2003 Elsevier Science B.V. All rights reserved.

*Keywords:* Agglomeration; Growth; Impurities; Discriminant factorial analysis

## 1. Introduction

Industry is more and more required to manufacture powders with defined properties in terms of size and morphology. These characteristics can be related to end-use properties such as filterability of slurry, flowability in storage tanks, bioavailability of pharmaceutical molecules, dissolution rate in a solvent, etc.

Many of those powders are produced by precipitation or crystallisation. Although widely studied, the later process is still far from being well understood. Yet, it is used largely from food industry and pure chemical processes to high technology electronic components and arts-related sciences like photography. In the sugar refining process, it is the most important step and, therefore, is worth every attempt to try to better understand it. The purpose is to grow sucrose crystals with a required standard of quality, essentially measured by the purity, by the shape, by the size distribution and by the visual aspect of the grain population. Sucrose is primarily a food

but is also included in the formulation of many pharmaceuticals.

Sucrose crystallisation occurs through mechanisms of nucleation, growth and agglomeration that are known to be affected by several operating conditions [1], of which the presence of impurities is mostly relevant. Agglomeration, in particular, is an undesired phenomenon to a large extent not yet understood, which has significant effect on the crystal size distribution and on the crystal aspect, i.e. on the final product quality. On one hand, agglomeration enables to obtain quickly large crystals, on contrary to nucleation, which favours small crystals. But on the other hand, due to the spreading of the size distribution, the separation of crystals from the liquid phase is more difficult. Uniform and well-formed large crystals are preferred, as they are easier to dry by centrifugation [2]. Agglomeration may result in a decrease of purity due to solution entrapment into the agglomerates. Such inclusions of dilute molasses are difficult to remove and increase the risk of bacterial contamination and poor storage behaviour [2]. The search for efficient methods for population characterisation, in terms of shape, perfect crystal and agglomerate contents and size distribution, is thus linked both to the scientific interest of understanding fundamental mechanisms of the crystallisation process and to the relevant practical interest of daily production requirements.

\* Corresponding author. Tel.: +33-3-83-17-52-77; fax: +33-3-83-17-53-26.

E-mail address: Marie-Noelle.Pons@ensic.inpl-nancy.fr (M.N. Pons).

Sucrose crystals present a rather complex structure of surfaces. Fig. 1 represents one of the possible combinations of its three-dimensional shape [3]. There is no agreement between authors about a theoretical ideal habit. Depending on the operating conditions, namely the presence of impurities, the growth kinetics of the different faces will vary [2,4–6]. The result is a diversification of crystal shapes. If a crystal is agglomerated, this phenomenon is not so important as the overall shape and size of the crystal is already highly modified. However, the impact of impurities such as dextran, which is the major soluble polysaccharide found in cane sugar, on the morphology of simple crystals may be extremely important [4,5]. It affects not only global growth kinetics but also the properties of the resulting solid product. It is easy to understand that a crystal with an elongated shape does not have the same mechanical properties as a more compact one.

In this work, procedures based on image analysis are proposed, which allows the quantification of not only size distributions but also of morphology distributions. Particles are observed by optical microscopy. Morphology is first assessed by a set of shape descriptors, namely related to particle silhouette elongation, circularity, robustness and concavity. In a second step, the particles are sorted into shape classes. Different classification methods can be applied such as discriminant factorial analysis [7], neural networks [7,8] and bayesian classifiers [8]. Discriminant factorial analysis has been used here. As an outcome of this classification, a degree of agglomeration is calculated for each crystal. Finally, a more detailed analysis of the shape of mono-crystals is proposed. The procedures are applied to commercial beet and cane sugar crystals as well as to crystal populations obtained in a lab-scale reactor in presence of different impurities.

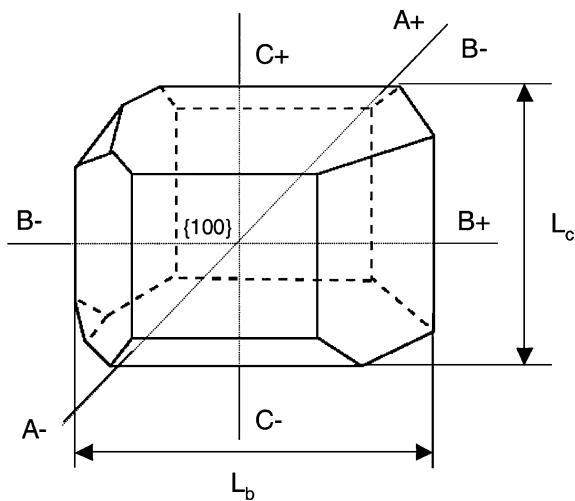


Fig. 1. Three-dimensional representation of one of the possible forms of a sucrose crystal [3].

## 2. Experimental methods

Brown cane and white beet sugars were purchased from a local store. White cane sugar was provided by RAR (Porto, Portugal). Dextran (molecular weight range:  $5 \cdot 10^6$  to  $40 \cdot 10^6$ ), raffinose ( $C_{18}H_{32}O_{16} \cdot 5H_2O$ ) and sodium carbonate were purchased from Sigma (St. Louis, MO) and glucose ( $C_6H_{12}O_6 \cdot H_2O$ ) from Prolabo (Paris, France).

Lab-scale crystallisation were run in a 20-l jacketed and mechanically stirred reactor equipped with a draft tube. A marine-type propeller was used for mixing. The stirring speed was set at 200 rpm. The reactor temperature was controlled by means of a water bath. The reactor medium was prepared by dissolution of commercial white beet sugar in osmosed water at  $60^\circ C$ . The Brix, Bx (mass percentage of solids in solution) calculated from Eq. (1) was adjusted at  $72^\circ$  Brix.

$$Bx = 396.74n_D - 511.54 \quad (R^2 = 0.99) \quad (1)$$

where  $n_D$  is the refractive index, as measured by a hand refractometer (ATAGO N-3000E) and  $R^2$  is the correlation coefficient. For calibration, commercial sucrose was mixed with water on a weight basis. The solution was kept at a temperature  $10^\circ C$  higher than the theoretical saturation temperature for several hours under stirring prior to measurement.

When needed, the impurity (raffinose, glucose, calcium carbonate or dextran) was added at this stage. The seed (commercial icing sugar [50%] in suspension in ethanol [50%]) was added (seed suspension volume = 0.2 ml) when the supersaturation  $\sigma$  reached 1.05. The temperature  $T$  was regularly adjusted to maintain the supersaturation at 1.05. The supersaturation was defined as

$$\sigma = \frac{Bx}{100 - Bx} \bigg/ \left( \frac{Bx_{sat}}{100 - Bx_{sat}} \cdot S_{sat} \right) \quad (2)$$

where  $Bx_{sat}$  is the Brix at saturation of the pure solution

$$Bx_{sat} = 64.447 + 8.222 \times 10^{-2}T + 1.66169 \times 10^{-3}T^2 - 1.558 \times 10^{-6}T^3 - 4.63 \times 10^{-8}T^4 \quad (3)$$

$S_{sat}$  is the coefficient of saturation and is a function of the impurities to water ratio in the solution

$$S_{sat} = a \frac{M_i}{M_w} + b + (1 - b) \exp \left( -c \frac{M_i}{M_w} \right) \quad (4)$$

where  $M_i$  and  $M_w$  are, respectively, the mass of impurities and of water, and  $a$ ,  $b$  and  $c$  are parameters only function of the type of impurities [9,10]. However, in the experiments presented here,  $S_{sat}$  was always in the range 0.95–1 and the effect of impurities on  $\sigma$  was neglected.

On termination of each run, the crystals are harvested, separated from the liquid by filtration on paper, washed twice with pure ethanol and dried.

### 3. Morphology assessment

#### 3.1. Image analysis

The crystals are deposited on a glass slide and observed by transmitted light microscopy with a Dialux20 (Leitz, Wetzlar, Germany) microscope equipped with a monochrome camera (Hitachi ICCTV) connected to a Matrox Meteor board on PC. Grey-level images (8-bit) of  $768 \times 576$  square pixels are captured. Several slides can be used to image the required number of crystals. Images are manually focused to have a good definition of the crystal contour line and the interior, from the point of view of the operator. The grabbing of one image takes about 15 s. These images are then treated, analysed and several numerical descriptors are extracted for each crystal using Visilog<sup>TM</sup> 5 (Noésis, les Ulis, France). There are two different procedures. The first one refers to the calculation of the 2D shape parameters that describe the silhouette of the particles and the second procedure applies to the calculation of a special pseudo 3D parameter.

Before performing the 2D measurements, the images are transformed through the following set of operations:

- thresholding—the number of grey levels of the image is reduced from 256 to 2 by an automated procedure based on the variance of the grey-level histogram [11] (Fig. 2a–b);

- hole filling (Fig. 2b–c);
- noise elimination (Fig. 2c–d);
- elimination of the objects that contact the board of the image (Fig. 2d–e);
- identification of the particles in the image (Fig. 2e–f).

The 2D size and shape descriptors are silhouette surface  $S$  from which the equivalent diameter ( $D_{eq} = 2\sqrt{S/\pi}$ ) is deduced, Crofton perimeter  $P$  [11], Feret diameters distribution, from which the maximal ( $F_{max}$ ) and minimal ( $F_{min}$ ) diameters are deduced to give size measurements of the particle, “length” and “breadth”, respectively (Fig. 3a). The Feret diameter in orientation  $\alpha$  is the distance between two parallels tangent to the silhouette and making an angle  $\alpha$  with the vertical. When the silhouette convex bounding polygon  $H_c$  (Fig. 3b) is rectangular,  $F_{max}$  measures the diagonal length and  $F_{min}$  the smallest side length. The following secondary parameters are calculated: circularity ( $C = P^2/4\pi S$ ), elongation ( $F_{max}/F_{min}$ ) and aspect ratio ( $F_{max}/D_{eq}$ ). The particle silhouette is compared to  $H_c$  (Fig. 3c): the particle robustness ( $\Omega_1$ ), its index of largest concavity ( $\Omega_2$ ), the ratio of the largest concavity to the total concavity ( $\Omega_3$ ) and its projected surface concavity index ( $CI = S/S_c$ , where  $S_c$  is the surface of  $H_c$ ) are deduced [12].

The pseudo 3D parameter that is calculated takes advantage of the transparency of sugar crystals to evaluate the complexity of its upper face and interior. When light is transmitted through the crystal, the beam is subject to phenomena of reflection and refraction at the crystal/air interfaces but also at the interfaces between two crystal planes in agglomerates. In the case of a mono-crystal, a unique zone with high grey levels is visible at the centre of the crystal (Fig. 4a). In the case of agglomerates, many

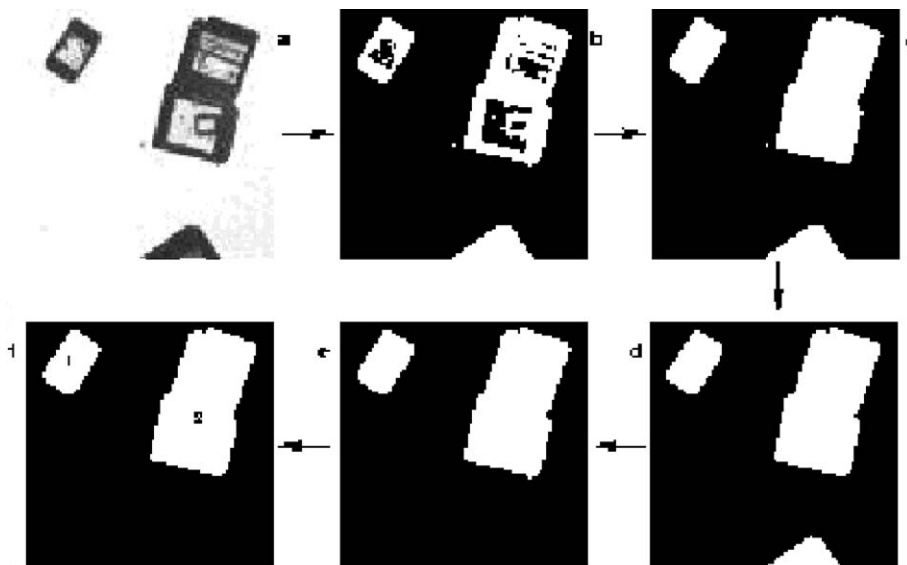


Fig. 2. Sequence of operations performed on images before extraction of the measurements.

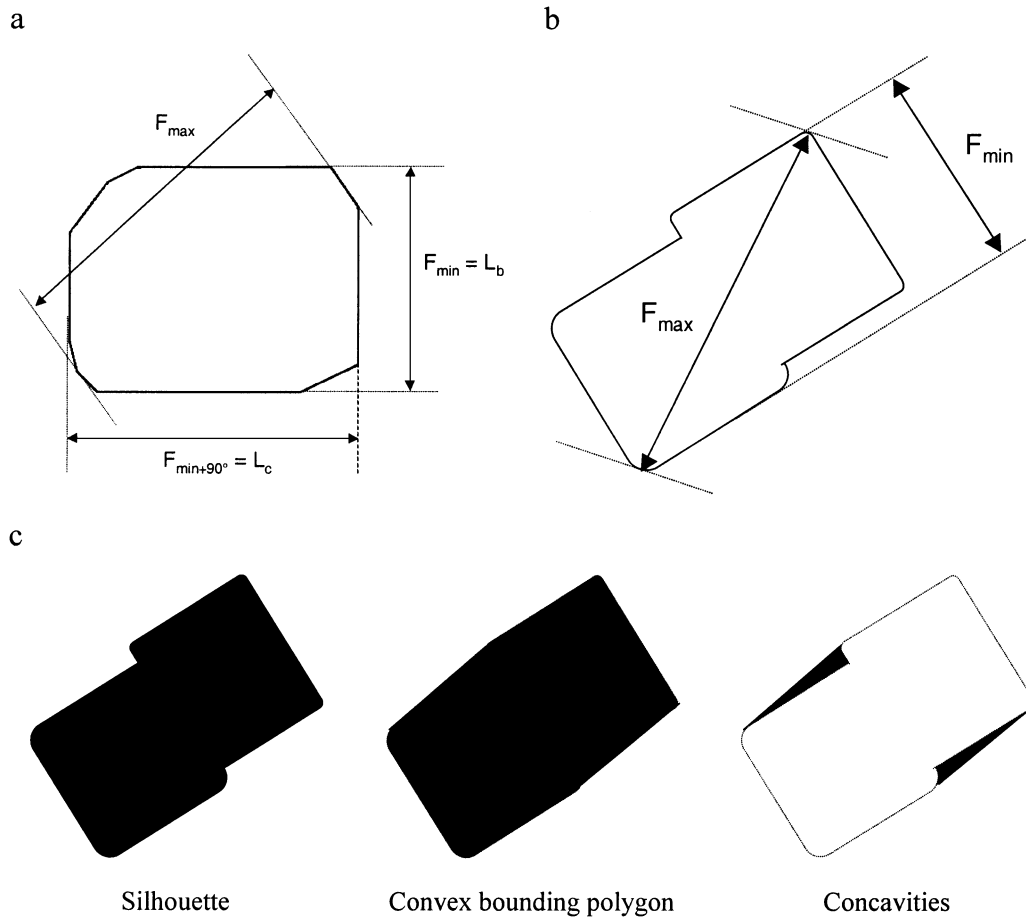


Fig. 3. Measurements on a convex (a) and concave (b) particle; (c) steps for the quantification of concavities.

internal zones are noticeable (Fig. 4e). The number of zones ( $N$ ) can be a criterion for the discrimination between simple crystals ( $N=1$ ) and agglomerates ( $N>1$ ). To improve the contrast between the internal zones and

the rest of the crystal, enhancement is performed by applying morphological transformations. The definition of morphological transformations is beyond the scope of this paper, but details can be found in Refs. [11] and [13].

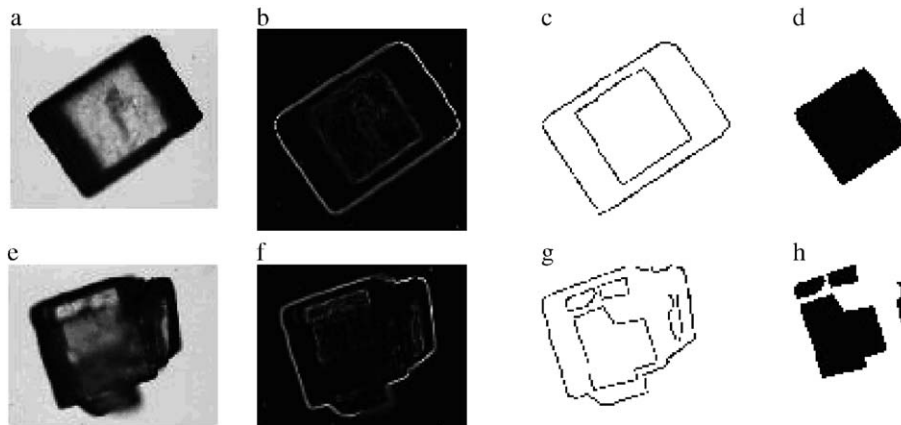


Fig. 4. Extraction of the pseudo-3D parameter: original image of a simple crystal (a) and an agglomerate (e); inner edges enhancement (b, f); threshold (c, g); identification of internal zones (d, h).

The first step is based on the fact that an image  $I$  is always lying between its eroded  $E(I)$  and its dilated  $D(I)$ :

$$E(I) \leq I \leq D(I) \tag{4}$$

For each pixel  $I(n,m)$  of the initial grey-level image  $I$ , the output grey level value  $O(n,m)$  will be the closest value of  $I$  between  $E(I)$  and  $D(I)$ :

$$O(n,m) = \begin{cases} D(I(n,m)) & \text{if } [D(I(n,m)) - D(n,m)] < [E(I(n,m)) - D(n,m)] \\ E(I(n,m)) & \text{otherwise} \end{cases} \tag{5}$$

In the second step, the morphological gradient of  $O$  is calculated, as the difference between its dilated  $D(O)$  and its eroded  $E(O)$  thresholded and combined with the silhouette to produce an image with the internal zones separated into one or several parts (Fig. 4d,h).

### 3.2. Crystal classification

Although the goal of the present technique is to automatically classify sugar crystals according to their degree of

agglomeration, several sets of crystals have first been visually classified. These are used both to train the statistical method employed and to assess the degree of agreement between the visual and automated classifications.

The crystals are separated into four groups as shown in Fig. 5. The groups were defined and agreed upon by several experts, according to their own rules of valuation of the degree of agglomeration of sugar crystals. These groups represent an increasing degree of crystal complexity as seen through the optical microscope. Simple crystals ( $S$ ) are supposed to be mono-crystalline. The complexity of agglomerates increases from small ( $SA$ ) to medium ( $MA$ ) then large ( $VA$ ). The crystal size was not considered as a parameter in the crystal classification, and for this reason, the scale has not being indicated of the images presented in this paper.

The automated classification of the crystals has been performed by a discriminant factorial analysis (DFA) method [14,15]. A statistical toolbox, Xlstat (T. Fahmy, Paris, France), running under Excel (Microsoft) was used for that purpose. In the first stage (training), a reference set of crystals is given to the classifier with indications of the shape class, as assigned visually by the expert. The software calculates the characteristics of each class in terms of its

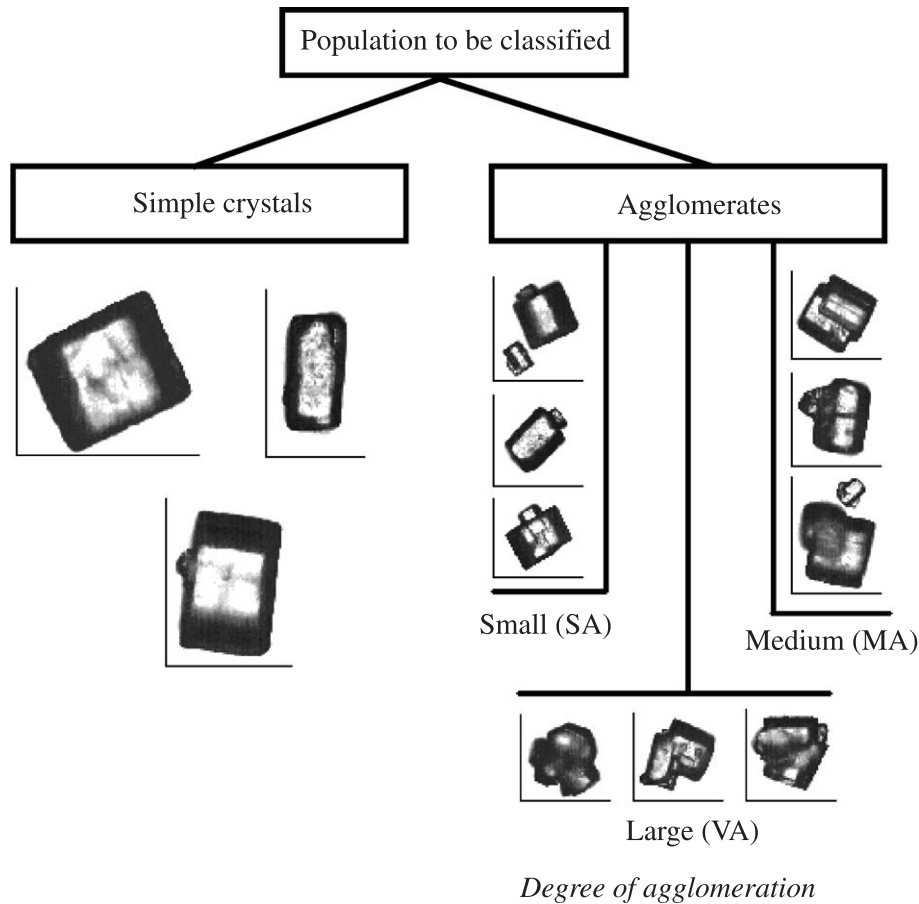


Fig. 5. Classification tree of sucrose crystals.

Table 1  
Comparison of classification rates for different shape descriptor sets for lab-crystallised particles

Descriptor set	PI (%)	Classification rate for S crystals (%)
Elongation, aspect ratio, circularity	84	76
$\Omega_1$ , $\Omega_2$ , CI	87	95
Elongation, aspect ratio, circularity, $\Omega_1$ , $\Omega_2$ , CI	87	92

centroid and variance radius. The operator has not to define numerically the limits of each class in terms of descriptor values. The distance of a crystal to the centroid characterises the probability for a crystal to belong to the class and is used as classification criterion for the subsequent stage. In this next stage, a second set (set to be tested) is proposed to the classifier, which assigns the crystal to the shape class based on the probability of crystal  $i$  to belong to one of the groups  $j$  ( $P_{b_{ij}}$ ), where  $\sum_j P_{b_{ij}} = 1$ . Each crystal is assigned to the group for which the probability is the highest.

The degree of mismatch (Eq. (6)) is used to grade the quality of the automated classification.

Performance Index = PI(%)

$$= \left( 1 - \frac{\text{Number of misclassified crystals}}{\text{Total number of crystals}} \right) \times 100 \quad (6)$$

Table 1 compares the classification results obtained on a set of 392 lab-crystallised particles for different descriptor sets. The information on concavities is extremely valuable when agglomerates are present: in the particles set under test these agglomerates represent 90% of the population in number. Even for simple crystals, a better classification rate is obtained by considering the full descriptor set. The increase in computation burden when nonconventional shape parameters such as  $\Omega_1$ ,  $\Omega_2$  and CI are taken into account has been judged worthwhile. Due to the continuous improvement in computer speed, it is not reasonable to give a precise calculation time. It was nevertheless less than 10 s per image on the computer used throughout this study.

Table 2 presents the results obtained for the binary classification (simple crystals/agglomerates) with two sets

Table 2  
Binary classification performance for white cane sugar crystals

Reference set	Test set	Use of $N$	Misclassified agglomerates	Misclassified simple crystals	PI (%)
$P_1 + P_2$	$P_1 + P_2$	Yes	34	5	89.6
$P_1 + P_2$	$P_1 + P_2$	No	40	6	87.8
$P_1$	$P_2$	Yes	9	5	90.2
$P_2$	$P_1$	Yes	30	1	86.8
$P_1$	$P_2$	No	9	6	89.4
$P_2$	$P_1$	No	33	4	84.2

Table 3  
Complete classification performance for white cane sugar crystals

Ref. set	Test set	PI (%)				
		S	SA	MA	VA	Binary
$P_3$	$P_3$	94.1	65.2	50	61.2	93.9
$P_3$	$P_4$	100	59.3	40	41.3	94.4

of white cane sugar crystals from the same initial population:  $P_1$  (171 agglomerates, 63 simple crystals) and  $P_2$  (107 agglomerates, 35 simple crystals). The variables considered are elongation, aspect ratio, circularity,  $\Omega_1$ ,  $\Omega_2$ ,  $\Omega_3$ , CI and  $N$ . The performance index decreases when the size of the reference set decreases: a larger error is obtained when  $P_2$  is the reference set. The use of  $N$  improves significantly the classification. However, it cannot be based solely on this parameter.

The determination of  $N$  is restricted to the case when crystals are sufficiently transparent: as a matter of fact,  $N$  cannot be obtained on brown cane sugar crystals. Another restriction comes from the fact that a greater magnification is required to determine  $N$  than the one necessary to obtain only the silhouette: as a result, to examine the same number of crystals, the number of images to analyse is larger. Working with a lower magnification can make the full automation of the image-grabbing phase much easier. For those reasons, the subsequent results were obtained without considering  $N$ .

Table 3 presents the results obtained for the complete classification with two sets of white cane sugar crystals,  $P_3$  (224 crystals) and  $P_4$  (180 crystals), from the same initial population. The variables considered are elongation, aspect ratio, circularity,  $\Omega_1$ ,  $\Omega_2$  and CI.

The discrimination between simple and agglomerates is satisfactory. In any case, the simple crystals are well recognised. Within the agglomerate group, discrepancies are high between two adjoining classes (SA and MA, MA and VA). This was also noticed on the lab-crystallised particles used to produce the results of Table 1. The classification made by the expert is based on the initial grey-level image when the automated classification is based

Table 4

Morphology distributions for different populations of sugar crystals:  $P_5$  = white beet sugar,  $P_6$  = brown cane sugar; visual = as classified by the expert, auto = automated classifier

Set	S (%)	SA (%)	MA (%)	VA (%)	Global degree of agglomeration (%)
$P_3$ (visual)	31.9	21.1	19.3	27.7	68.1
$P_3$ (auto)	35.7	25.8	17.4	21.1	64.3
$P_4$ (visual)	34.4	17.8	22.3	25.5	65.6
$P_4$ (auto)	39.7	26.6	19.6	14.1	60.3
$P_5$ (visual)	41.4	20.4	16.1	22.1	58.6
$P_5$ (auto)	54.3	14.8	21.6	9.3	45.7
$P_6$ (visual)	54.8	14.8	7.8	22.6	45.2
$P_6$ (auto)	55.4	16.8	14.2	13.6	44.6

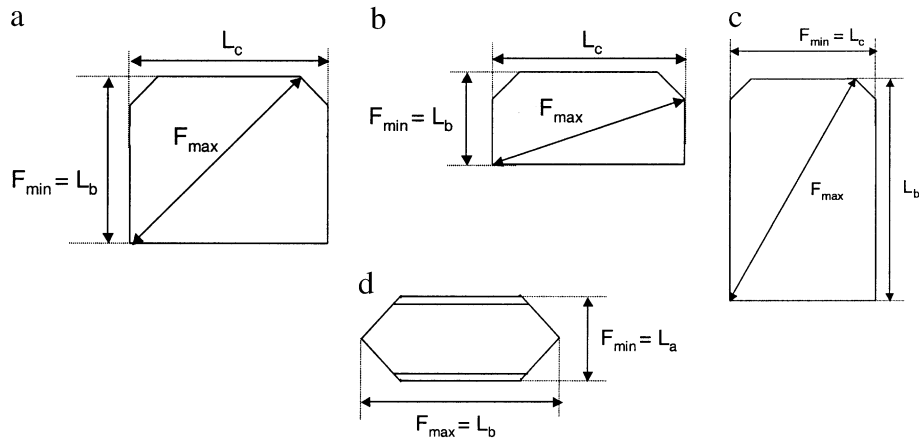


Fig. 6. Some of the frequent shapes observed with sucrose mono-crystals: (a) prototype of type A sucrose crystal (crystal 2), (b) + dextran (crystal 3), (c) + raffinose (crystal 4), (d) prototype of type B (crystal 5).

solely on the silhouette, which explained most of the discrepancies. Furthermore, the classification made by the experts is not absolute: the performance index between two experts on the morphology distribution of set  $P_3$  was 92%, which is very similar to the value obtained by automated classification.

Table 4 gives the morphology distributions obtained for the different commercial sugars. For  $P_4$  and  $P_5$ , the reference set was  $P_3$ . For the brown sugar, as the crystals do not have the same morphology as the white sugar crystals, a new and appropriate reference set was selected. The reference set for the white beet sugar crystals  $P_5$  was  $P_3$ , which explains the larger difference in the visual and automated classifications of  $P_5$ : it could be seen visually that the beet sugar agglomerates are slightly different from the white cane sugar ones. This stresses out the necessity to choose an appropriate refer-

ence set. As it will be shown later, impurities affect the shape of the crystal. Impurities in cane and beet sucrose solutions are different. For that reason, it is better to build a reference set in agreement with the nature of the raw material.

There is compensation between classes, which explains why the agreement is better between the visual and the automated classifications than it could be deduced from the examination of Table 3. The automated classification behaves similarly for the commercial and the lab-crystalised particles.

### 3.3. Degree of agglomeration

Using the results provided by the DFA method, it is possible to numerically quantify the degree of agglomeration of each crystal,  $Ag_i$ . If the four probabilities are taken

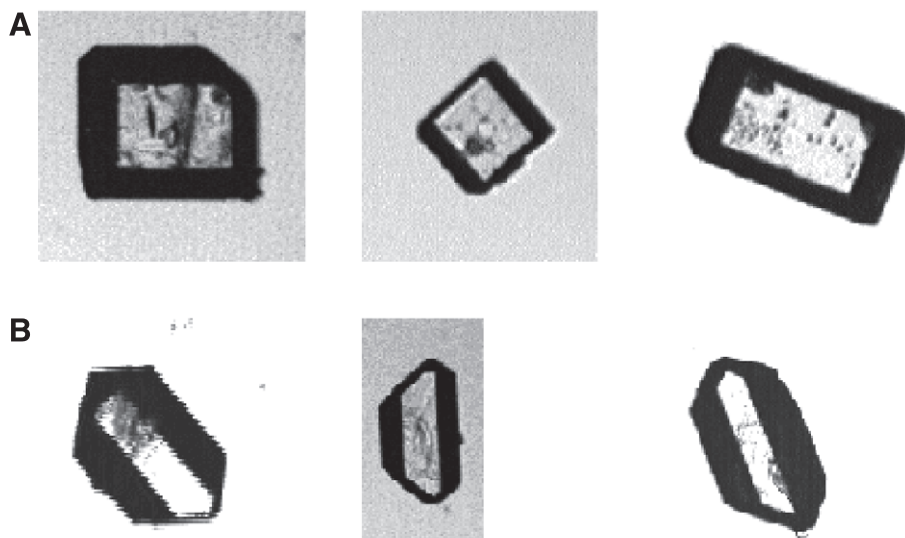


Fig. 7. The two different shapes of mono-crystals identified, A and B.

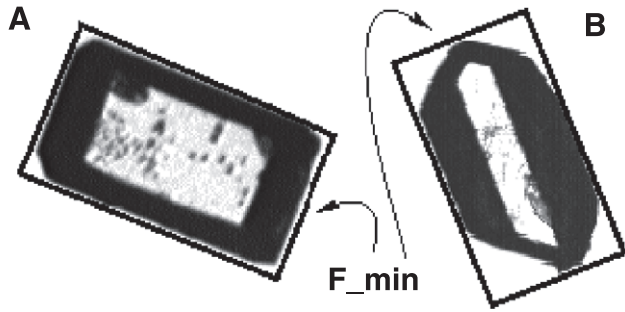


Fig. 8. Calculation of the  $Box_{ratio}$  parameter.

into account and not just the largest one,  $Ag_i$  can be calculated using Eq. (7).

$$Ag_i = 100 \left( Pb_{i,S} + \frac{4}{3}Pb_{i,SA} + \frac{5}{3}Pb_{i,MA} + 2Pb_{i,VA} - 1 \right) \quad (7)$$

This relation is a linear combination of the four probabilities calculated so that

$$Pb_{i,S} = 1 \Rightarrow Ag_i = 0\%; \quad Pb_{i,SA} = 1 \Rightarrow Ag_i = 33\%; \quad Pb_{i,MA} = 1 \Rightarrow Ag_i = 67\%; \quad Pb_{i,VA} = 1 \Rightarrow Ag_i = 100\%.$$

### 3.4. Habit of mono-crystals

Once the crystals have been classified as simple or agglomerates, it would be interesting to further characterise mono-crystals according to their shape. It is a challenge because, as stated previously, the number of observed shapes is high and the projected silhouettes of the simple crystals have many axes of symmetry. Fig. 6a presents one of the most frequent habits in commercial sugar. Elongation of the *C*-axis by dextran and of the *B*-axis by raffinose gives rise to the shapes of Fig. 6b,c, respectively [2]. These three crystals lay on one of their faces parallel to the BC plane.

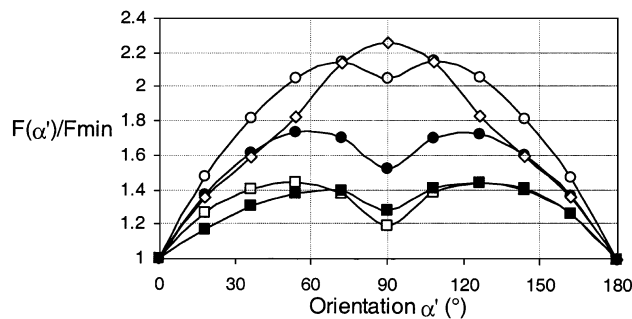


Fig. 9. Variation of the normalised Feret diameters in function of orientation for crystals 1 (■), 2 (□), 3 (◇), 4 (●) and 5 (○).

Table 5  
Characteristics of sucrose mono-crystals

Crystal	$L_b/L_c$	$L_a/L_b$	$S_{box}/S$	$F_{max}/F_{min}$
1 (Fig. 1)	0.79	–	1.06	1.44
2 (Type A)	0.84	–	1.03	1.45
3 (+ Dextran)	0.49	–	1.05	2.16
4 (+ Raffinose)	1.52	–	1.02	1.73
5 (Type B)	–	0.44	1.30	2.27

When the crystals are deposited on a glass surface to be observed under the optical microscope, they tend to land on their largest face so as to attain the highest mechanical stability. The crystal depicted in Fig. 6d was also largely observed in our experiments and lays on a face

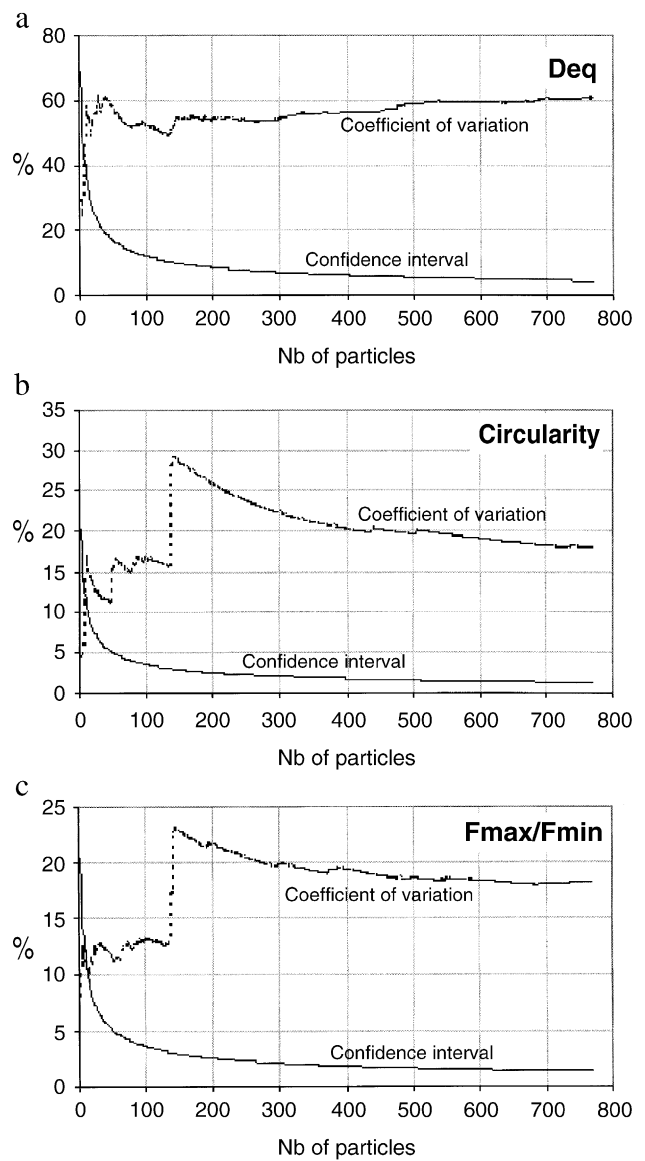


Fig. 10. Variation of the reduced confidence interval at 95% (—) and the coefficient of variation (---) in function of the number of particles for (a)  $Deq$ , (b) circularity  $C$  and (c)  $F_{max}/F_{min}$ .

parallel to the AB plane. The recognition of the crystal shape based on the analysis of the contour was initially thought of. However, due to the high number of potential shapes to identify, it demands a well-defined contour with a large magnification of each crystal. This would be very time-consuming for an industrial application. A simpler procedure was developed with the aim to classify the crystals as of type A (Fig. 7a) or type B (Fig. 7b). In order to distinguish between these two different shapes, some additional parameters have been introduced.

From Fig. 4d, it is possible to calculate the surface occupied by the central and transparent part of the crystal  $S_{in}$ . The ratio between the surface of the crystal and this

interior part ( $Area_{ratio} = S/S_{in}$ ) tends to be larger for crystals of type B.

It can be seen in Fig. 6 that one of the characteristic lengths of the simple crystal can be obtained directly from  $F_{min}$ . It is not so with  $F_{max}$ . Due to shape of the convex bounding polygons of the crystals depicted in Fig. 6, the Feret diameter at  $\alpha = \alpha_{min} + 90^\circ$  ( $F_{min+90^\circ}$ ), where  $\alpha_{min}$  is the tangent orientation corresponding to  $F_{min}$ , gives a second characteristic length. However, it should be noticed that without any additional information, it is not possible to determine to which length ( $L_a$ ,  $L_b$  or  $L_c$ )  $F_{min}$  and  $F_{min+90^\circ}$  correspond, respectively. Types A and B crystals can be included in a rectangle of surface  $S_{box} = F_{min} \cdot F_{min+90^\circ}$  (Fig.

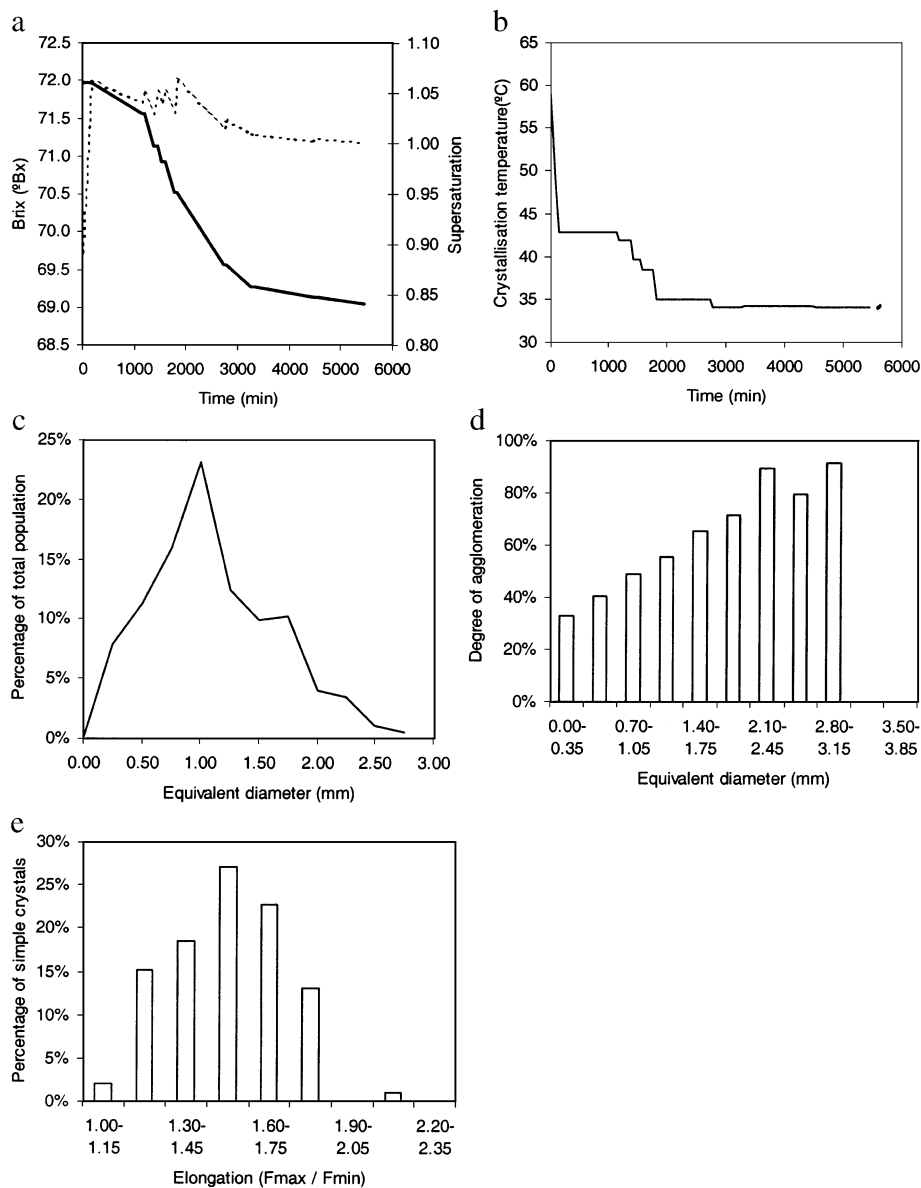


Fig. 11. Crystallisation of pure sucrose: Brix (—) and supersaturation (---) (a) and solution temperature (b) in function of time; (c) size distribution; (d) degree of agglomeration in function of size; (e) elongation of simple crystals.

8). The ratio between this surface and the surface of the crystal ( $\text{Box}_{\text{ratio}} = S_{\text{box}}/S$ ) is higher for type B crystals, as they do not fit so well within the rectangular box.

Besides these two parameters, the particle elongation ( $F_{\text{max}}/F_{\text{min}}$ ) and a set of Feret diameters calculated at 20 different angles between  $0^\circ$  and  $180^\circ$ , with an angular step of  $9^\circ$ , are used to distinguish between the two types of simple crystals. In order to make the Feret diameters independent of the crystal size, they are normalised by  $F_{\text{min}}$ . Fig. 9 represents the variation of the normalised Feret diameters ( $F(\alpha')/F_{\text{min}}$ ) with respect to  $\alpha' = \alpha - \alpha_{\text{min}}$  for the different crystals of Figs. 1 and 6, while the shape ratios are given in Table 5. Crystal 5 (Type B) has a  $F(\alpha')/F_{\text{min}}$  curve that presents a different pattern from the ones of crystals 1–4 (type A). As expected,  $\text{Box}_{\text{ratio}}$  for crystal 5 is much higher than for the other crystals. Using the DFA method based on the value of these parameters for each simple crystal, it is possible to automatically assign it in one of the two groups, A or B. It should be noticed again that the size is not here again a criterion for shape classification.

In order to evaluate the success of the automated classification, a set of 305 simple crystals were visually and automatically classified. These crystals were isolated from the images of four different populations. The DFA method was trained using two of these populations (170 crystals)

and the other two were used to validate the classification. The total number of misclassified crystals was seven, that is the degree of agreement between the visual and automatic classification ( $PI$ ) was 98%. As previously, the operator does not have to select the limit values of the descriptors for A and B groups.

### 3.5. Number of particles

The choice of the number of particles to examine is always a key issue with image analysis. On one hand, a large number of particles increase the accuracy of the morphological characteristics of the sample. On the other hand, the larger the number, the longer the time necessary for visualisation, image capture and treatment, especially when the microscope stage is not automated [16].

To test the effect of the particle number on the results, a test has been performed on a set of 770 crystals. Fig. 10 presents the variations of the reduced confidence interval at a level of significance of 5% (i.e.  $100 \times$  confidence interval at 95%/average value, where the confidence interval of the mean is based on the Student law with a significance level of 5%) and the coefficient of variation (i.e.  $100 \times$  standard deviation/mean value) for three parameters:  $D_{\text{eq}}$ ,  $C$  and  $F_{\text{max}}/F_{\text{min}}$ . A minimum of 500 particles should be analysed

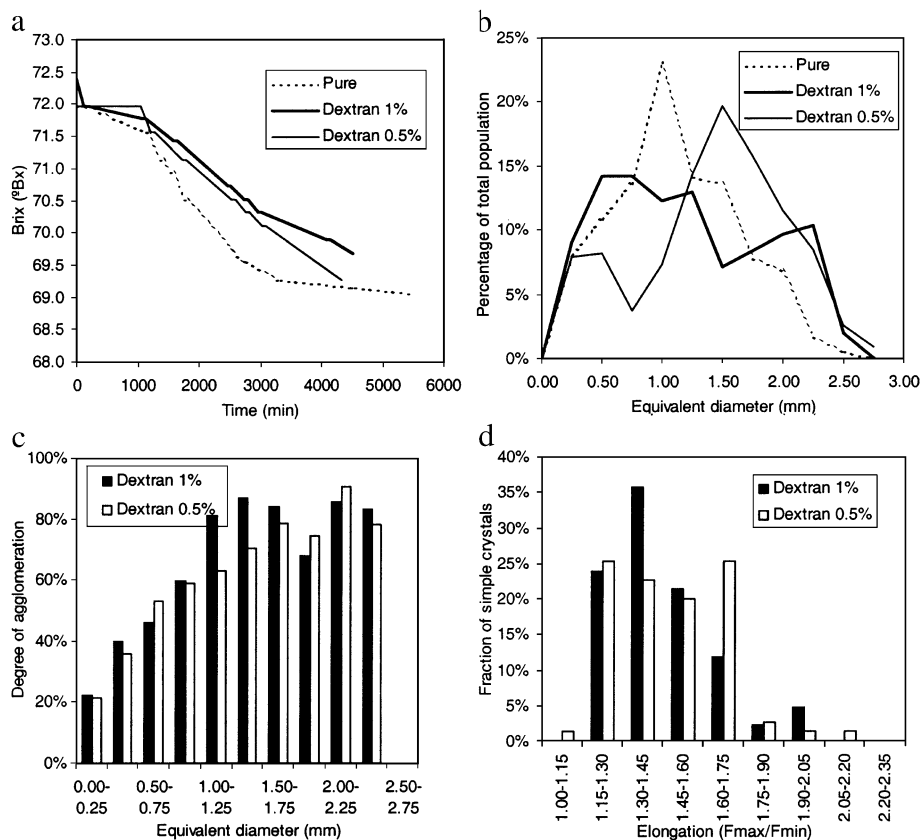


Fig. 12. Crystallisation of sucrose in presence of dextran: (a) Brix in function of time; (b) size distribution; (c) degree of agglomeration in function of size; (d) elongation of simple crystals.

to insure a reduced confidence interval smaller than 5% for  $D_{eq}$  and 2% for the shape descriptors and an acceptable stability of the coefficients of variation, i.e. of the parameters distributions. The stabilisation of the coefficients of variation is obtained with a larger number of particles than the one of the mean values. In Fig. 10, the effect of the change of slide around 150 particles can be seen on the coefficients of variation.

#### 4. Experimental results

The previously described procedures have been used to investigate the effect of impurities on the quality of sugar crystals.

The first experiment was performed with a pure sucrose solution. The other six runs contain a certain amount of a given pure chemical species that are dextran (0.5 wt.% and 1 wt.%), raffinose (0.5 wt.% and 1 wt.%), glucose (1 wt.%) and sodium carbonate (0.1 wt.%). The image analysis procedure is applied to 150–250 images for each experiment, resulting in the study of more than 500 particles.

##### 4.1. Crystallising from a pure sucrose solution

The results obtained for the pure sucrose solution are summarised in Fig. 11. The control of supersaturation by manual adjustment of the bath temperature is delicate, but the Brix decreases regularly (Fig. 11a). As seen in Fig. 11d, the agglomeration degree increases with the size of the crystal. It is important to remember that large crystals have spent a longer time in the solution than smaller ones, thus increasing the probability of becoming agglomerates. The average elongation parameter for simple crystals is 1.60, which is a little larger than the value found for the “ideal” crystal 1. Sixty percent of the simple crystals are of type A. The average degree of agglomeration is 48%.

##### 4.2. Influence of dextran

Dextran is a polymer present in the sugar cane. Its main consequence to the sugar refining process is the increase of the viscosity of the solutions. Slower rates of crystallisation are observed as seen in Fig. 12a. An enlargement of the overall size distribution can be seen in Fig. 12b in presence

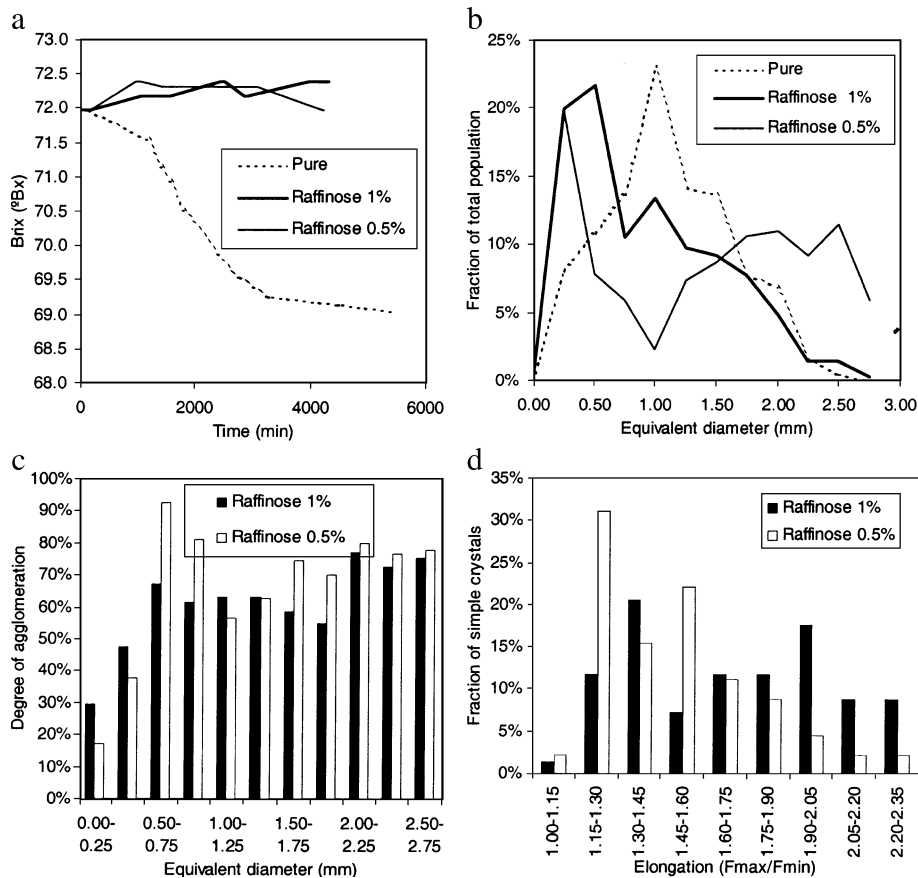


Fig. 13. Crystallisation of sucrose in presence of raffinose: (a) Brix in function of time; (b) size distribution; (c) degree of agglomeration in function of size; (d) elongation of simple crystals.

of dextran. The average degree of agglomeration increases with the impurity concentration: 53% for 0.5% and 56% for 1%, which is higher than with the pure sucrose solution (Fig. 12c). There is no evident relationship between the concentration of dextran and the percentage of simple crystals of type A: 53% with 0.5% but 67% with 1%, when it is 60% with 0% dextran. Elongated crystals were expected with this impurity according to Chen [2]. On the contrary, as shown in Fig. 12e, the average elongation is smaller than with the pure solution: 1.52 (for 0.5%) and 1.44 (1%). However, some very elongated crystals can be spotted: 2% and 5% of the simple crystals exhibit elongation values larger than 2.9 with 0.5% and 1% dextran, respectively. This reduced effect could be due to the fact that the dextran present in the solution is not native and that its concentration is low [4,5].

### 4.3. Influence of raffinose

A rapid inspection of Fig. 13a immediately reveals a very strange behaviour: in presence of raffinose, the solution Brix did not decrease as expected but increased. It will be shown later that raffinose is a very strong inhibitor of sucrose

growth kinetics. Considering that a solution at 72° Bx contains practically 72% of sucrose and 28% of water, a small change in the sugar content does not change much its Brix. On the other hand, a small amount of evaporated water (the experiments lasted for 3 days) provokes an increase of the Brix.

Fig. 13b reveals a crystal size distribution for the raffinose systems rich in small crystals when compared to the results obtained with a pure solution. This means that either the nucleation kinetics is higher or the growth kinetics is lower than in the pure sucrose system. As the total amount of crystallised sucrose is very low, it is reasonable to assume that raffinose is a strong sucrose growth inhibitor.

The average degree of agglomeration is similar to the one obtained with dextran: 62% and 51% with 0.5% and 1% raffinose, respectively. The variation of the degree of agglomeration with respect to size (Fig. 13c) is different, however, it seems to be more homogeneous over the size distribution.

Raffinose also changes the crystal habit. Simple crystals are more elongated in its presence than those obtained with a pure sucrose solution, and they are predominantly of type B (60–65%). As indicated by Chen [2], raffinose induces an

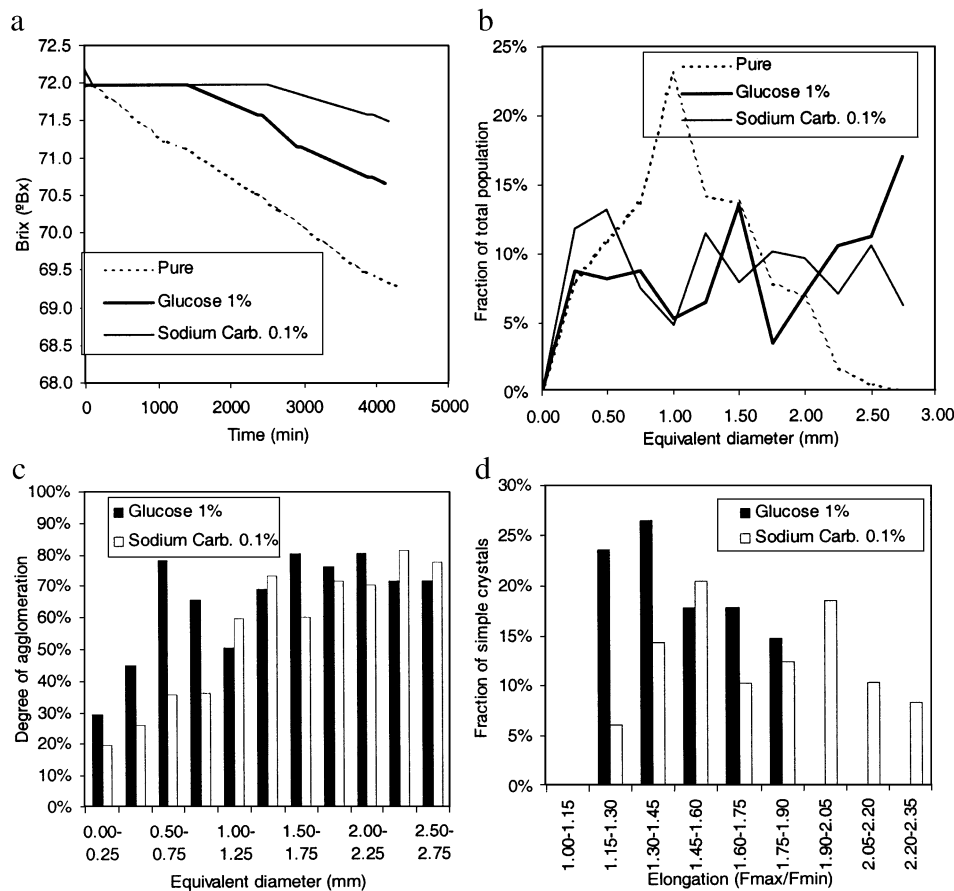


Fig. 14. Crystallisation of sucrose in presence of glucose and sodium carbonate: (a) Brix in function of time; (b) size distribution; (c) degree of agglomeration in function of size; (d) elongation of simple crystals.

elongation of the  $B$ -axis. However, it is delicate to draw deeper conclusions, as the number of simple crystals was limited in these experiments.

#### 4.4. Influence of glucose and sodium carbonate

Glucose is a by-product of sucrose. It results from its decomposition and is present in all sucrose-water systems. Sodium carbonate is introduced in the system during the refining process. Although most of it is separated before the crystallisation stage, a significant amount may still reach this phase. It is important to note that the amount of sodium carbonate used in this experiment is only 0.1%. All other experiments have been carried out with concentrations of impurities of 0.5% and 1%. Sodium carbonate is a very strong inhibitor of sucrose crystallisation kinetics (Fig. 14a), and with a higher concentration of this salt, it was impossible to obtain enough crystals. Glucose is also an inhibitor of sucrose crystallisation kinetics, although not as strong as sodium carbonate.

Both glucose and sodium carbonate provoked a spread of the crystal size distribution (Fig. 14b). In the case of glucose, this may be due to a decrease in the growth kinetics as the degree of agglomeration is high even for small crystals, as with raffinose. Crystal growth would then be due to agglomeration and not to sucrose transfer from the solution to the crystals.

In the case of sodium carbonate, the same cannot be said, as the degree of agglomeration is lower than in the pure sucrose system for almost all crystal size classes. The conclusion is that sodium carbonate blocks all crystallisation mechanisms, including agglomeration.

Glucose produces mostly type A simple crystals (57%) with an average elongation of 1.57, similar to the value obtained for pure sucrose (Fig. 14d). Even a very small amount of sodium carbonate causes a strong elongation of the simple crystals that are mostly of type A (72%).

## 5. Conclusions and perspectives

Using image analysis techniques, it is possible to obtain valuable information on the size and morphology of sucrose crystals. The information collected is not easily accessible through any other technique, namely the evaluation of the degree of agglomeration and the shape descriptors. The quantification of crystal size is also more reliable as it is done by a direct “visual” measurement on crystals. The procedures have been kept as simple as possible to promote their use in an industrial environment: the crystals are visualised by optical microscopy and the image analysis is fully automated.

The chemical species used as impurities in the system have various effects on the crystallisation kinetics and on the properties of the crystal populations. Dextran presented the lowest impact and sodium carbonate the highest. Even at a

concentration 5 to 10 times lower than the other impurities tested, sodium carbonate practically stopped the crystallisation process and the crystals that did manage to appear had the most abnormal shapes. All tested impurities caused a slowdown of the kinetic rate of one or another of the crystallisation mechanisms. Dextran showed a slight impact on the nucleation rate, raffinose strongly reduced the growth rate, glucose and sodium carbonate reduced both nucleation and growth rates although the effect of sodium carbonate was much stronger. Although not dramatic, an effect of impurities on agglomeration was noticed. It is not so much the average degree of agglomeration that was modified, but mostly the variation of the agglomeration with respect to the size that presents different patterns.

The classification of mono-crystals according to their shape produced puzzling results, which might have several explanations. A more detailed classification might be necessary, which is difficult because the number of possible shapes is high and because the contour of real crystals is not as perfectly defined as in theory. The number of mono-crystals is probably not sufficient to draw full conclusions. If a limit of 500 particles is sufficient to have a global view of the size and shape distribution of a sample, a larger number should in fact be analysed in order to have a meaningful number of individuals in the different shape classes.

In future work, this aspect will be considered. The introduction of newly measured variables such as the degree of agglomeration should allow a better understanding of the crystallisation phenomena and of their implication for designing particles presenting specific end-use properties.

#### Symbols

$a, b, c$	coefficients
$Ag_i$	degree of agglomeration of crystal $i$
$Area_{ratio}$	ratio of the crystal surface to its interior transparent part
$Box_{ratio}$	ratio of the Feret box surface to the crystal projected surface
Bx	Brix
$C$	circularity
CI	concavity index
$D(I)$	image resulting from the morphological dilation of $I$
$D_{eq}$	equivalent diameter
$E(I)$	image resulting from the morphological erosion of $I$
$F_{max}$	maximal Feret diameter
$F_{min}$	minimal Feret diameter
$F_{min+90^\circ}$	Feret diameter perpendicular to $F_{min}$
$H_c$	convex bounding polygon
$I$	grey-level image
$L_a, L_b, L_c$	reference crystal side lengths
$M_i$	mass of impurity
$M_w$	mass of water
$N$	number of internal zones
$(n,m)$	pixel position with respect to line $m$ and row $n$ in an image
$n_D$	refractive index

$O$	grey-level image, output from a morphological transformation
$P$	Crofton perimeter
$Pb_{i,j}$	probability for crystal $i$ to belong to shape group $j$
PI	performance index
$R^2$	correlation coefficient
$S$	projected surface
$S_{\text{box}}$	Feret box surface
$S_c$	surface of $H_c$
$S_{\text{in}}$	surface of transparent zone
$S_{\text{sat}}$	coefficient of saturation
$T$	temperature
$\alpha$	tangent orientation
$\sigma$	supersaturation
$\Omega_1$	robustness
$\Omega_2$	largest concavity index
$\Omega_3$	concavity ratio

### Acknowledgements

This work was partially financed by the Ambassade de France au Portugal, program reference 98/B4/065, by program PRAXIS XXI/BD/5491/95 and by the Portuguese Foundation for Science and Technology—contract POCTI/1999/EQU/33131.

### References

- [1] L.J. Kuijvenhoven, L.M. De Pree, E.J. De Jong, Conglomerate formation in sugar crystallization: Part I. Effect of process conditions, *Int. Sugar J.* 85 (1983) 201–207.
- [2] J.C.P. Chen, Raw sugar quality criteria, *Cane Sugar Handbook*, Wiley, New York, 1993, pp. 343–374.
- [3] Z. Bubnik, P. Kadlec, Sucrose crystal shape factors, *Zuckerindustrie* 117 (1992) 345–350.
- [4] D.N. Sutherland, Dextran and crystal elongation, *Int. Sugar J.* 70 (1968) 355–358.
- [5] D.N. Sutherland, N. Paton, Dextran and crystal elongation: further experiments, *Int. Sugar J.* 71 (1969) 131–135.
- [6] M. Saska, Calculated form of the sucrose crystal, *Int. Sugar J.* 85 (1983) 259–261.
- [7] B. Bernard-Michel, S. Rohani, M.N. Pons, H. Vivier, H.S. Hundal, Classification of crystal shape using Fourier descriptors and mathematical morphology, *Part. Part. Syst. Charact.* 14 (1997) 193–200.
- [8] A. Zaknich, Characterization of aluminium hydroxide particles from the Bayer process using neural network and Bayesian classifiers, *IEEE trans. Neural Netw.* 8 (1997) 919–931.
- [9] V. Jesic, Variables affecting saturation coefficient in cane final molasses, *Int. Sugar J.* 79 (1977) 274–277.
- [10] G. Vavrinecz, Formation and composition of beet molasses: I. The equation for solubility, *Sugar Technol. Rev.* 6 (1978) 117–129.
- [11] C.R. Russ, *The Image Processing Handbook*, CRC Press, Boca Raton, 1995.
- [12] M.N. Pons, H. Vivier, J. Dodds, Particle shape characterization using morphological descriptors, *Part. Part. Syst. Charact.* 14 (1997) 272–277.
- [13] M. Coster, J.L. Chermant, *Précis d'analyse d'images*, 2nd ed., CNRS, Paris, 1989.
- [14] B.F.J. Manly, *Multivariate Statistical Methods*, 2nd ed., Chapman & Hall, 1994.
- [15] M. Otto, *Chemometrics*, Wiley-VCH, Weinheim, 1999.
- [16] M.N. Pons, H. Vivier, V. Delcour, J.R. Authelin, L. Paillères-Hubert, Morphological analysis of pharmaceutical powders, *Powder Technol.* 128 (2002) 276–286.